AIAA JOURNAL
Vol. 44, No. 7, July 2006

Inviscid Model of the Formation of a Rotor Tip Vortex

D. P. Pulla,* Vishwanath Godavarty,* O. R. Burgraff,† and A. T. Conlisk‡
The Ohio State University, Columbus, Ohio 43210-1107

The roll up of trailing vortex filaments shed from a finite-length rotor blade in hover has been computed and analyzed. It is shown that the formation of the tip vortex is a strong function of the aspect ratio of the blade, angle of attack, and number of blades. The amount of trailing circulation associated with the tip vortex develops downstream and approaches an asymptotic constant that is less than that the total amount of trailing circulation. The results for the vertical and horizontal velocity profiles downstream of the blade are compared with the results for an infinite blade and with the experimental results of McAlister et al. (McAlister, K., Tung, C., and Heineck, J. T., "Devices That Alter the Tip Vortex of a Rotor," NASA TM-2001-209625, Aeroflightdynamics Directorate, TR-01-A-003, Feb. 2001). The velocity profiles across the tip vortex compare extremely well with experiment.

Nomenclature

A	=	aspect ratio of the blade
a	=	blade radius
c	=	blade chord
n	=	number of blades
R	=	nondimensional radial coordinate $= r/\alpha$
r	=	dimensional radial coordinate
$\bar{r}$	=	core radius
u, v, w	=	nondimensional velocity components in the x, y, z directions, respectively
v_z	=	axial velocity induced by the vortex ring cylinder comprising the inboard sheet
W	=	nondimensional induced downwash on the blade
$\boldsymbol{X} = (x, y, z)$	=	nondimensional Cartesian coordinates
$\boldsymbol{X}' = (x', y', z')$	=	position vector of the points on the vortex in Eq. (15); coordinates of the stationary reference frame on Fig. 5
$\bar{y}, \bar{z}$	=	y and z components of the center of the tip-vortex core
α_e	=	effecive angle of attack
α_0	=	geometric angle of attack
Γ	=	dimensional bound circulation
γ_θ	=	circulation per unit of axial length along the vortex cylinder
λ	=	parameter involving aspect ratio, angle of attack, and number of blades
ψ	=	azimuthal angle traversed by the blade from its initial position at rest
Ω	=	angular velocity of rotation of blades

Introduction

THE tip region of a rotor blade is composed of a complex vortical three-dimensional flowfield. Because there must be zero circulation at the tip, vorticity is created within the boundary layer on the blade and convected into the wake. This trailing vorticity creates the trailing vortex system. The complex flow in the tip region has a major influence on the blade performance. The purpose of this paper is to present results extending the work of Li et al.[1] to the case of finite-aspect-ratio rotor blades.

Despite the fact that at first glance viscous terms in the governing equations must be included in any calculations, experimental work by several authors[2,3] has shown little dependence on the blade Reynolds number. This means that under these conditions inviscid methods can be used to describe the origin and evolution of the tip vortex and also to predict the circulation and velocities in the tip region, provided some sort of method is employed to account for a vortex core. If the vortex core is accounted for, the character of the swirling velocity field within the tip vortex, typical of what is seen in the Lamb vortex distribution, is predicted by these pseudo-inviscid methods. The results of the comparison with the experimental data of McAlister et al.[4] bear this out.

Experimental data suggest that the the formation of the tip vortex is dependent on what is called the vortex Reynolds number defined by $Re = Re_B(C_T/\sigma)$, where C_T is the thrust coefficient, σ is the rotor solidity, and Re_B is the blade Reynolds number.[5] This is not surprising because the thrust coefficient is highly dependent on the strength of the tip vortex. The dependence is particularly strong when going from model-scale to full-scale rotors; the experimental data cited by the authors for model scale indicate that all of the vortex Reynolds numbers are within a factor of about 10. Because the primary motive is to understand model-scale vortex development, we do not consider the effect of vortex Reynolds number. This dependence can be explored in a later paper.

Navier–Stokes computations of the rotor wake are time consuming and expensive, and usually involve the specification of a turbulence model. Moreover, the tip vortex loses structure caused by numerical error after a rotor phase angle of about 90 deg. Thus Navier–Stokes solvers are most often used to predict global properties such as blade loads in steady state, and many codes have performed well for model-scale rotors.[6]

Many researchers have investigated the fixed-wing trailing vortex wake including Batchelor,[7] McCormick et al.,[8] Brown,[9] Moore and Saffman,[10] Francis and Kennedy,[11] McAlister and Takahashi,[12] Dacles-Mariani et al.,[13] Devenport et al.,[14] and Christopher and Lyle.[15] As noted by Francis and Kennedy,[11] vortex formation begins to occur almost at the leading edge of the wing. This results in the picture of the tip vortex as a collection of vortex-like lines shed from those discrete positions on the wing, which appear helical in nature as depicted in the photograph in Fig. 1 (Ref. 16); these streak-line patterns show the behavior of trailing vortices shed from those discrete positions and illuminate the region around the vortex core; note that some of the vortex-like lines wrap from the underside. Such a filament-like structure for the tip vortex is mentioned by Lanchester[17] indicating a long history of this interpretation. However, no computational model of the tip vortex incorporating a model of this type has been constructed (Fig. 1).

Typical of Navier–Stokes calculations for a fixed wing is the work by Dacles-Mariani et al. Dacles-Mariani et al.[13] report solutions for

Received 11 August 2005; revision received 17 January 2006; accepted for publication 17 January 2006.

*Graduate Research Assistant, Department of Mechanical Engineering.
†Professor, Department of Mechanical Engineering.
‡Professor, Department of Mechanical Engineering. Associate Fellow AIAA.

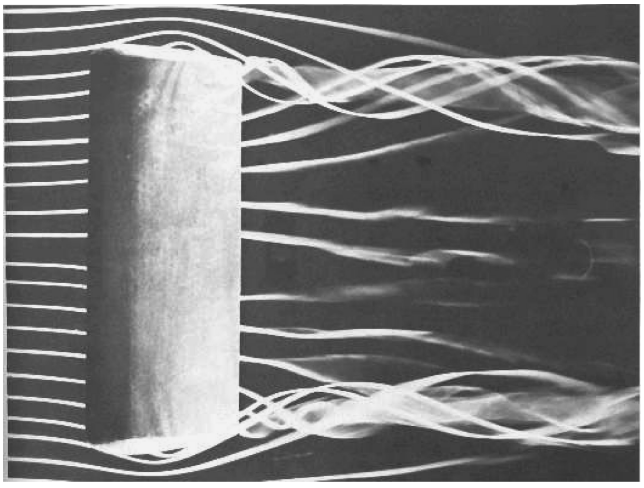

Fig. 1 Vortex wake of a fixed wing as photographed by Head.[16]

the fixed wing in which up to one million points with grid clustering have been used. They report that they could resolve the outer portion of the vortex but could not resolve the viscous portion of the core owing to large numerical diffusion.

Roger[18] used a second-order Euler method together with an adaptive-grid solver to study the tip-vortex flowfields around NACA 0015 airfoil. The predicted results for the surface pressures and integrated lift agree well with experiments. However, the core radius is larger, and the peak induced tangential velocity behind the wing is less than the experimental data. This appears to be caused by large numerical diffusion in the numerical approximation.

There have been a number of Navier–Stokes calculations of the rotor wake in the last several years, and several papers have focused on the formation of the tip vortex. Srinivasan and Baeder[19] present tip-vortex particle paths showing a braiding phenomenon similar to that depicted on Fig. 1. High-order differencing schemes have also been used.[20,21] In that work the swirl velocity prediction for the ninth-order scheme preserves the amplitude of the tip vortex fairly well. They note that in addition to using higher-order methods it is necessary to align the grid with the principle flow direction. For all problems considered, the ninth-order scheme was considerably more accurate than a fifth-order scheme.

Many experimental investigations have focused on the wakes of helicopter rotor blades, and a survey of these results is presented by Conlisk.[6,22] Bhagwat and Leishman[3] use a three-component laser Doppler velocimetry to study the tip-vortex flowfield. The measurements show that the strength of the tip vortex is about 83–85% of the maximum bound circulation, whereas the remaining is contained in the inner vortex sheet and our results validate these measurements as shown later. Earlier, Cook[23] suggested that the tip-vortex circulation is much less than the maximum bound circulation. However, Caradonna and Tung[24] suggest that the tip-vortex circulation is close to the maximum bound circulation.

Because of the scarcity of detailed data on the origin of the tip vortex, McAlister and his colleagues[4] have conducted a series of experiments on a single-bladed rotor. McAlister et al.[4] have measured the fully three-dimensional velocity field for a rigid finite-span rotor blade; the measurements include data at three and six chord lengths downstream of the trailing edge of the rotor blade, where the origin of the tip vortex in particular can be analyzed. According to McAlister et al.,[4] the vortex begins to form near the point of maximum thickness on the top of the blade. The center of the vortex is offset inboard a small amount, and the circulation within the vortex varies with the rotor phase angle. The vortices leave the wing in the chordwise direction at the trailing edge as in the case when the classical Kutta condition is applied. One of the objectives of this work is to compare the detailed experimental results for the two velocity components characterizing the vortex in a vertical plane slicing across the vortex. It will be shown that the present finite-blade computations compare much better than previous work described by Li[1] for the lifting line.

The major objective of this paper is to present improved inviscid calculations of the formation of the tip vortex that can be used to accurately predict the velocity field near the blade tip. The downstream development of the rotor tip vortex behind a finite blade is described, and the results are compared with those for an infinite blade.[1] Li[1] focused on the large-aspect-ratio rotor blade and presented a numerical solution for the leading-order term in an asymptotic series in inverse aspect ratio for the formation of the tip vortex. They found that in the tip region where the bound circulation varies rapidly the individual vortex segments roll over each other and form a strong tip vortex. The tip vortex does not completely roll up near the rotor as assumed by many wake models; instead, the tip vortex develops downstream, and its circulation seems to be approaching a constant, which appears to be significantly less that the maximum bound circulation. However, more work needs to be done to confirm this point.

In this paper results for a low-aspect-ratio blade are presented. Dimensional analysis shows that there is a single parameter involving the number of blades, angle of attack, and aspect ratio, which governs the development of the tip vortex. In the course of the solution, the circulation, asymptotic core radius, and velocity profiles are predicted as a function of downstream distance from the blade. A single-bladed rotor for which experimental data exist has been considered; the results compare very well with the experiment validating the inviscid flow assumption, and it is shown that the lifting-line model does not do as well in comparing with experimental data.

Inboard Sheet Model

It is well known that the rotor wake consists of a tip-vortex system coupled with a relatively weaker inboard vortex sheet. The inboard sheet consists of line vortices that trail all across the rotor as a result of the variation of the bound circulation, forming an approximately cylindrical slipstream filled with concentric helical vortices. These discrete helical vortices can be approximated by uniform cylindrical sheets of vorticity. To compute the downwash, it is assumed that these elemental vortex cylinders can be viewed as composed of vortex rings, whose strength is approximately constant on each cylinder. The axial component of the helical vortices, that is, the component of the circulation oriented in a direction normal to the tip-path plane, can be ignored because it does not contribute to the downwash.

A cylindrical coordinate system (r, θ, z) is convenient, where r is the radial coordinate, θ the azimuthal coordinate, and z the axial coordinate. (See Fig. 2, which illustrates a single vortex cylinder.) These elemental vortex cylinders, formed from the inboard vortex sheet, are superposed with the vortex cylinder generated by the tip vortex to form the complete rotor slipstream.

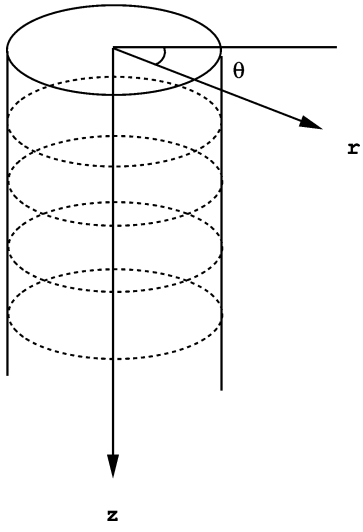

Fig. 2 Sketch of the cylindrical coordinate system.

For a single cylinder of vortex rings of circulation γ_θ per unit of axial length along the cylinder, it has been shown previously by Radcliff et al.[25] that the axial velocity induced by the vortex ring cylinder using the Biot–Savart law is given by

$$v_z(r) = \begin{Bmatrix} \gamma_\theta/2 & \text{for} & r < r' \\ \gamma_\theta/4 & \text{for} & r = r' \\ 0 & \text{for} & r > r' \end{Bmatrix} \tag{1}$$

Now these elemental vortex-ring cylinders, formed from the inboard vortex sheet, are superposed with the vortex cylinder generated by the tip vortex to form the complete rotor slipstream. Because the downwash at radius r in the rotor plane is induced only by those cylinders of larger radius, the net downwash is given by

$$v_z(r) = \frac{1}{2}\int_r^a \gamma_{\theta i}(r')\,\mathrm{d}r' + \frac{1}{2}\gamma_{\theta t} \tag{2}$$

where the subscripts i and t refer to the inboard vortex sheet and to the tip vortex, respectively.

The circulation per unit length γ_θ is estimated by smearing out each successive loop of the vortex helix over the distance it advances in one turn of the rotor. The time for one revolution is $2\pi/\Omega$, where Ω is the angular velocity of the rotor. The distance the vortex at radius r is swept downward in one rotor revolution is then $2\pi v_z/\Omega$. Let Γ be the value of the bound circulation along the rotor. Then the strength of the shed circulation per unit length along the rotor is $-\mathrm{d}\Gamma/\mathrm{d}r$, and hence the vorticity of the cylindrical sheet at radius r for n blades is

$$\gamma_\theta(r) = -\frac{n\Omega}{2\pi v_z(r)}\frac{\mathrm{d}\Gamma}{\mathrm{d}r} \tag{3}$$

The tip vortex is translated downward only by its own self-induced downwash because the interior vortex cylinders do not induce downwash at the tip. The downwash induced by a vortex cylinder at its own radius is only half that induced at interior points, so that from Eq. (1) the downwash at the tip is just $\gamma_{\theta t}/4$. Hence one loop of the tip vortex winds a distance downward:

$$\Delta_z = 2\pi v_z(a)/\Omega = \pi\gamma_{\theta t}/2\Omega$$

and so the strength of the tip vortex cylinder for n blades, corresponding to the circulation Γ_t at the tip for each blade, is just

$$\gamma_{\theta t} = n\Gamma_t/\Delta_z = 2n\Gamma_t\Omega/\pi\gamma_{\theta t}$$

Solving for $\gamma_{\theta t}$ gives the result

$$\gamma_{\theta t} = \sqrt{(2n/\pi)\Gamma_t\Omega} \tag{4}$$

We use the flat-plate value for the lift coefficient and then find for the circulaton

$$\Gamma = \pi u_\infty c\alpha_e$$

where u_∞ is replaced by Ωr for the rotor in hover, and α_e is the effective angle of attack

$$\alpha_e = \alpha_0 - v_z/\Omega r$$

Here α_0 is the geometric angle of attack of the airfoil section. Combining these results gives

$$\Gamma(r) = \pi\Omega c[\alpha_0 r - (1/\Omega)v_z(r)] \tag{5}$$

For simplicity, both chord c and geometric angle of attack α_0 are assumed to be constant across the blade radius. Then from Eq. (3), the vorticity of the inboard vortex cylinders is given by

$$\gamma_\theta(r) = -\frac{n\Omega^2 c}{2\,v_z(r)}\left[\alpha_0 - \frac{1}{\Omega}\frac{\mathrm{d}v_z}{\mathrm{d}r}\right] \tag{6}$$

Substituting this expression for γ_θ into Eq. (2) yields the integrodifferential equation for the induced downwash

$$v_z(r) = -\frac{n\Omega^2 c}{4}\int_r^a \left[\alpha_0 - \frac{1}{\Omega}\frac{\mathrm{d}v_z(r')}{\mathrm{d}r'}\right]\frac{\mathrm{d}r'}{v_z(r')} + \sqrt{\frac{n\Gamma_t\Omega}{2\pi}} \tag{7}$$

Here Γ_t is given in terms of v_z at the tip by Eq. (5).

The simplicity of the solution can be more easily recognized by use of the following nondimensional variables. Let

$$R = r/a, \qquad W(R) = v_z(r)/\Omega a\alpha_0, \qquad \lambda = \alpha_0 a/nc \tag{8}$$

Then with Γ_t evaluated as $\Gamma(a)$ from Eq. (5), Eq. (7) takes the simpler form

$$W(R) = -\frac{1}{4\lambda}\int_R^1 \left[1 - \frac{\mathrm{d}W(R')}{\mathrm{d}R'}\right]\frac{\mathrm{d}R'}{W(R')} + \sqrt{\frac{1}{2\lambda}[1 - W(1)]} \tag{9}$$

It is clear from Eq. (9) that the solution for the downwash function W depends on the radius function R and only the one aspect-ratio parameter λ. The integrodifferential equation can be converted to an ordinary differential equation simply by differentiating term by term and collecting terms in $\mathrm{d}W/\mathrm{d}R$; the nonlinear equation is reconfigured into standard form:

$$[1 + 4\lambda W(R)]\frac{\mathrm{d}W}{\mathrm{d}R} = 1 \tag{10}$$

Choosing the sign of the radical to require positive downwash (positive lift), the solution of the integral equation becomes

$$W(R) = (1/4\lambda)\left(\sqrt{1 + 8\lambda R} - 1\right) \tag{11}$$

(If the negative sign is chosen, the downwash is negative everywhere in $0 < R < 1$). The corresponding bound circulation distribution for an individual blade is obtained from Eq. (5):

$$\Gamma/\Omega a\alpha_0 = \pi c[R - W(R)] \tag{12}$$

The value of the downwash must be used to calculate the blade influence coefficients that force the velocity normal to the blade to be zero. For the case of an infinitely long blade, because the tip vortex formation region scales on the inverse aspect ratio this expression would be merely evaluated at $R = 1$. This is the problem solved by Li.[1] On the other hand, for the finite-blade case considered here the full expression must be kept.

Li[1] performed an asymptotic analysis valid for large aspect ratio A and defined an inner variable $Y = A(1 - R)$. Expanding the outer solution for the induced downwash in the rotor-tip path plane $W(R)$ with the inner variable $Y = A(1 - R)$, we find that to leading order, as $A \to \infty$, the solution for the downwash near the tip is

$$W(Y) \sim \sqrt{1 + 8\lambda}\Big/4\lambda - 1/4\lambda \tag{13}$$

For a rotor blade with finite aspect ratio, the preceding equation is written without ignoring the most significant higher-order terms as

$$W(Y) = \frac{1}{4\lambda}\left\{\sqrt{1 + 8\lambda}\left[1 - \frac{4\lambda A^{-1}Y}{1 + 8\lambda} - \frac{8\lambda^2 A^{-2}Y^2}{(1 + 8\lambda)^2} + \mathcal{O}(A^{-3})\right] - 1\right\} \tag{14}$$

Vortex Model

The present model of the rotor wake is a vortex method. The use of a vortex method to model the rotor wake goes back to the work of Scully,[26] who computed solutions for the rotor wake using a time-marching vortex method. The inboard vortex sheet was represented by a single large-core vortex located at midspan.

Modern relaxation methods are llustrated by the work in Ref. 27, which uses a linearized version of the Biot–Savart law. They were also able to obtain results for forward flight. A relaxation technique

that uses curved vortex elements to evaluate hover performance has also been described.[28,29] The blade is represented as a lifting surface. Compressibility effects are incorporated, and the drag coefficient is obtained from two-dimensional airfoil data, and results for a number of rotors are presented. Vortex methods are the dominant means for predicting the wake structure in comprehensive rotor codes. However, to date it is believed that such methods have not been consistently used to predict tip-vortex structure during its formation process.

In this paper we use a vortex method with a cutoff parameter to describe a given vortex filament. The cutoff parameter represents the influence of the vortex core flow on the flowfield and regularizes the Biot–Savart law. Such an approach is motivated by the work of Widnall et al.,[30] who show that the cutoff parameter can be determined by matching the outer inviscid and irrotational solution with an inner viscous region for a vortex ring. By assuming that a general vortex filament can locally be represented by a ring vortex, the cutoff parameter for the ring can be used in the general case, and in this paper we assume that the core is a Rankine vortex.

The vortex structure is assumed to be represented by the modified Biot–Savart law[30]

$$\boldsymbol{U}_V(s,t) = -\frac{1}{4\pi}\int_C \Gamma \frac{(\boldsymbol{X}-\boldsymbol{X}')\times(\partial \boldsymbol{X}'/\partial s')\,\mathrm{d}s'}{\{|\boldsymbol{X}-\boldsymbol{X}'|^2+\mu^2\}^{\frac{3}{2}}} \tag{15}$$

where μ is the cutoff parameter. The value of $\mu = a_v e^{-3/4}$ for a Rankine vortex, and this value has worked well in past work. It is the nonzero value of the cutoff parameter that captures the viscous nature of the core flow, and this can be seen in the discussion of empirical two-dimentional vortex models discussed previously.[3]

Figure 3 shows the discretization of the tip-vortex. All velocity integrals are evaluated at integration points that lie midway between adjacent advance points or at the center of a vortex filament as shown in Fig. 3. The total vortex-induced velocity is computed by adding the velocity contributions of all of the vortex segments. The velocity contribution due to each tip vortex segment is computed using the analytical formula given by Ref. 6 for a straight-line vortex

$$\boldsymbol{U}_v = \frac{\Gamma_a}{4\pi}\left\{\left[\frac{(|\boldsymbol{a}|+|\boldsymbol{b}|)(|\boldsymbol{a}||\boldsymbol{b}|-\boldsymbol{a}\cdot\boldsymbol{b})}{|\boldsymbol{a}||\boldsymbol{b}||\boldsymbol{a}\times\boldsymbol{b}|^2}\right]\right. \tag{16}$$

where $\boldsymbol{b}$ is the vector connecting the point P and $X'_{\mathrm{va,j+1}}$ while $\boldsymbol{a}$ connects P to $X'_{\mathrm{va,j}}$. Γ_a is the value of circulation of the vortex segment connecting $X'_{\mathrm{va,j}}$ and $X'_{\mathrm{va,j+1}}$. The evaluation point in the figure is shown as $X_{ve,j}$.

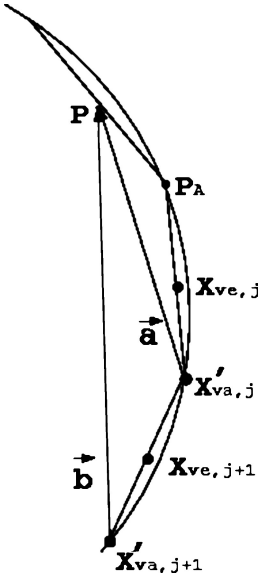

Fig. 3 Tip-vortex discretization using straight-line vortex filaments. X_{ve} and X'_{va} are evaluation and advance points, respectively.

Each advance point on the tip vortex is advanced in time by solving

$$\frac{\mathrm{d}\boldsymbol{X}_v}{\mathrm{d}t} = \boldsymbol{U} \tag{17}$$

where $\boldsymbol{X}_v$ is the position vector of a point on the vortex and $\boldsymbol{U}$ is the total velocity induced at that point. The solution is stepped in time using an Adams–Moulton scheme with a Runge–Kutta starting formula. The integral on the right-hand side of Eq. (17) is evaluated at advance points, whereas the integration of the first-order system of ordinary differential equation (17) is carried out using integration points. The integration points are located at the midpoint of each straight-line vortex segment.[31] After every time step, each of the advance points is moved to its new location. This method is observed to give better results than where the advance points and integration points coincide.[32]

Lifting Surface Model for a Finite Wing

The lifting surface model is described by Li,[1] and the geometry is depicted in Fig. 4. For clarity, in Fig. 4b only three chordwise panels and nine spanwise panels are shown, whereas in the numerical calculation one chordwise and 20 spanwise panels were used.

The bound vorticity varies rapidly close to the wing tip. Hence accurate computation of the bound vorticity requires a strong

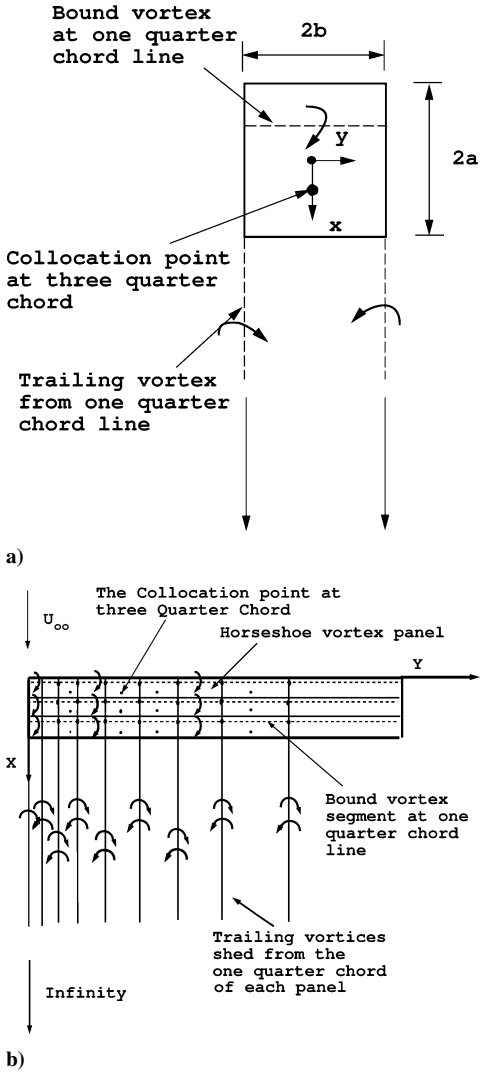

Fig. 4 Horseshoe-vortex panel implementation for a finite wing. The panel width is nonuniform in the spanwise direction, as discussed in the text. The velocity boundary condition is applied at the three-quarter chord line at the midspan point of each panel: a) definition of the local panel coordinates and b) definition of the global coordinates.

concentration of the horseshoe-vortex panels in the region near the wing tip. Consequently it is helpful to use panels of variable width. We have chosen the variation

$$Y = \bar{b}\tan\theta, \qquad 0 < \theta < \pi/2$$

where $\bar{b}$ is the computational span of the blade. Distributing the panels uniformly in the θ variable increases the density of panels near the blade tip.

Each blade panel consists of a horseshoe vortex system with a bound vortex along the panel quarter-chord line together with trailing vortices lying along the panel edges and extending through the trailing edge of the wing and moving with the local velocity after leaving the trailing edge of the wing to infinity downstream.

The boundary condition of zero normal velocity on the wing surface is satisfied at the three-quarter-chord point on the centerline of each panel,[33,34] and the vortices emanate from the panel quarter-chord line and extend through the trailing edge of the wing to infinity downstream (Fig. 4b).

Thus the dimensionless panel circulations $\Gamma_k, k = 1, \ldots, m$ can be evaluated from the surface boundary condition, expressed as the linear set of equations

$$\sum_{k=1}^{m} A_{jk}\Gamma_{bk} = -\alpha_0(1 - W_j), \qquad j = 1, \ldots, m \tag{18}$$

where W_j is the dimensionless induced downwash at the jth panel.

The rotor blade is modeled by a finite number of panels along the length (spanwise) and the width (chordwise) of the blade. As the number of panels in the spanwise direction is increased, more locations of the exact rollover position of the trailing vortices can be identified, which increases the accuracy of the plots. The effect of increase in the number of chordwise panels is very small as will be shown later. Here a variable panel width is used as in Li,[1] and the positions of the trailing vortices are calculated also as in Li.[1]

Tip-Vortex Trajectory

Having obtained the spanwise distribution of the bound circulation, the positions of the shed vortices behind the wing can be calculated. In a steady inviscid flowfield, the trailing vortex lines are also streamlines. The positions of vortex lines can be obtained relative to the blade or relative to the ground depending on the need. Let v be the velocity induced in the y direction and w be the velocity induced in the z direction relative to the blade. Let u be the pertubation from the freestream velocity in the x direction relative to the blade. The positions of the vortex lines relative to the blade can be obtained by solving the nondimensionalized equations

$$\frac{\mathrm{d}y}{\mathrm{d}x} = \frac{v}{1+u} \sim v \tag{19}$$

$$\frac{\mathrm{d}z}{\mathrm{d}x} = \frac{w + \sin\alpha_0}{1+u} \sim w + \sin\alpha_0 \tag{20}$$

where $u \ll 1$; an analysis of the numerical data reveals that $u \sim \mathcal{O}(10^{-}4)$ over the entire domain. Here x is the independent variable measured from leading edge of the wing, and all spatial variables are scaled on the chord. The variable x is the direction normal to and relative to the blade so that it can be identified with the arc length from the blade. The vortices are initiated at the one-quarter-chord position of each panel at the beginning of the numerical integration for every iteration. For the initial condition, $z = 0$, and y is the spanwise location of the trailing vortex shed from the one-quarter-chord of each panel. The trailing vortices are forced to stay on the wing surface up to the trailing edge of the wing but can be displaced in the y direction by the induced velocity. This set of ordinary differential equations was solved numerically by the Adams–Moulton method. Note that the velocity components were calculated for straight-line trailing vortices in the first iteration. The computed trajectories are the perturbations from the expected helical structure of the tip vortex in a steady-state configuration.

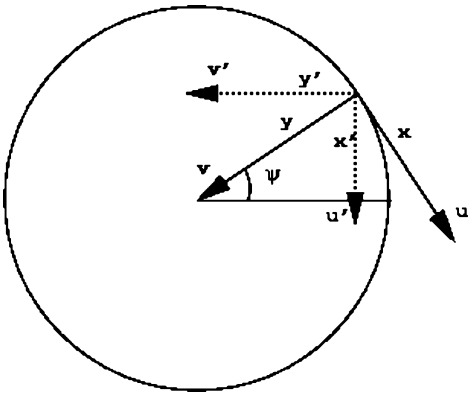

Fig. 5 Reference frame fixed to the blade (x', y', z') and the stationary reference frame (x', y', z') after the blade moves by an angle ψ from its initial position of rest.

The preceding equations (dimensionless) can be written in a stationary inertial coordinate system $(x',\ y',\ z')$ by introducing the parameter ψ, which is the azimuthal angle traversed by the blade relative to its initial position at rest. Both the preceding coordinate systems are shown in Fig. 5 after the blade traverses an azimuthal angle ψ. The velocity in the y' direction is $v\cos\psi - \sin\psi$, and that in the x direction is $v, \sin\psi + \cos\psi$. Hence the positions of the vortex lines relative to the inertial coordinate system can be obtained by solving the set of equations

$$\frac{\mathrm{d}y'}{\mathrm{d}x'} = \frac{v\cos\psi - (1+u)\sin\psi}{v\sin\psi + (1+u)\cos\psi} \sim \frac{v\cos\psi - \sin\psi}{v\sin\psi + \cos\psi} \tag{21}$$

$$\frac{\mathrm{d}z'}{\mathrm{d}x'} = \frac{w + \sin\alpha_0}{v\sin\psi + (1+u)\cos\psi} \sim \frac{w + \sin\alpha_0}{v\sin\psi + \cos\psi} \tag{22}$$

where the symbols v and w represent the y and z velocity components induced by the wake relative to the blade. Ω is the angular velocity of the blade.

To obtain the initial positions of the trailing vortices, three parameters are introduced to describe the roll-up process. They are $\bar{y}$, $\bar{z}$, which are the y and z components of the center of the tip-vortex core, and $\bar{r}$, which defines the core radius measured from the centroid. We define

$$\bar{y} = \frac{\sum_{k=1}^{n}\sum_{j=1}^{n_x}\Gamma_{j,k}y_{j,k}}{\sum_{k=1}^{n}\sum_{j=1}^{n_x}\Gamma_{j,k}} \tag{23}$$

$$\bar{z} = \frac{\sum_{k=1}^{n}\sum_{j=1}^{n_x}\Gamma_{j,k}z_{j,k}}{\sum_{k=1}^{n}\sum_{j=1}^{n_x}\Gamma_{j,k}} \tag{24}$$

where n is the number of trailing vortices, which are rolling over each other; n_x is the number of chordwise panels; and $\Gamma_{j,k}$ is the circulation of the panel (j, k). The core radius $\bar{r}$ has been defined as

$$\bar{r} = \sqrt{\frac{\sum_{k=1}^{n}\sum_{j=1}^{n_x}(\bar{y} - y_{j,k})^2 + (\bar{z} - z_{j,k})^2}{n \times n_x}} \tag{25}$$

The iterative process was assumed to be convergent when $\bar{r}_{\text{new}} - \bar{r}_{\text{old}}/\bar{r}_{\text{old}}$ is less than 10^{-4} at each given value of x. Here one chordwise panel and 20 spanwise panels have been used on the wing surface and 120 nodes on each of the trailing vortices. The separation between the nodes on each of the trailing vortices is 0.05. Beyond the last node, the trailing vortex is represented by a semi-infinite, horizontal straight vortex line extending to $x = +\infty$ and parallel to the freestream velocity.

Results

Finite-Aspect-Ratio Single-Bladed Rotor

The effect of varying the number of chordwise and spanwise panels in the blade model was analyzed for numerical accuracy.

Table 1 Experimental parameters in McAlister et al.[4] experiments

Parameter	Value
R	45 in. (1.14 m)
Ω	870 rpm
c	7.5 in. (0.19 m)
N	1

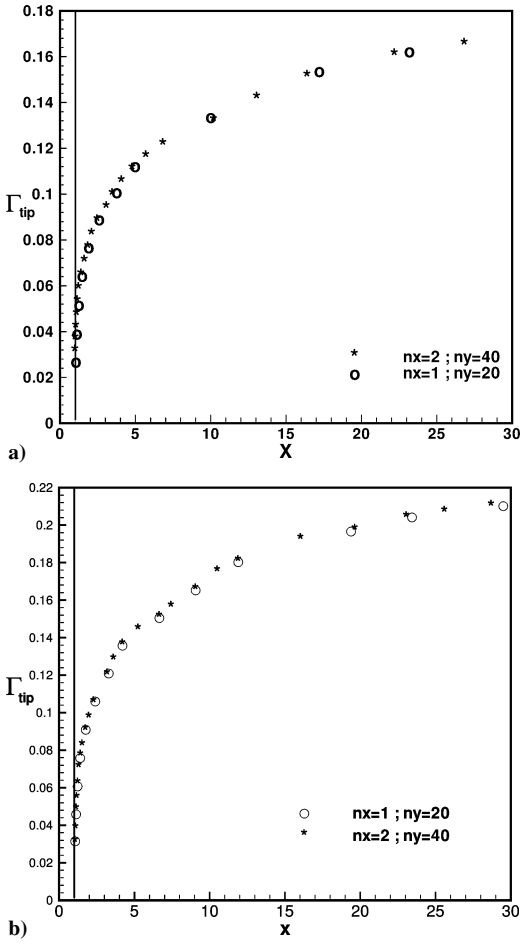

Fig. 6 Effect of variation in the number of chordwise and spanwise panels on the tip circulation of a single-bladed rotor: *, two chordwise panels and 40 spanwise panels and ○, one chordwise panel and 20 spanwise panels. The angle of attack is $\alpha = 8$ deg: a) Infinite-aspect-ratio blade and b) finite-aspect-ratio blade and $\lambda = 0.84$.

Figure 6 shows the growth of the tip-vortex circulation along x for a particular configuration with a different number of chordwise and spanwise panels for the case of an infinite-aspect-ratio and a finite-aspect-ratio single-bladed rotor. It is clearly seen that using one chordwise and 20 spanwise panels gives nearly the same result as that obtained using two chordwise and 40 spanwise panels. Thus, for all results presented in this work the rotor blade is represented by one chordwise and 20 spanwise panels. The calculation of the centroid of the tip vortex is converged out to 30 chord lengths beyond the leading edge of the blade in all of the results to be presented.

The experimental results for vertical and horizontal velocity profiles from McAlister et al.[4] were produced for a rotor blade with an aspect ratio of six. The experimental parameters are presented in Table 1. Figure 7 presents the top view of the roll-up process for a single-bladed rotor for $\alpha_0 = 8$ deg ($\lambda \sim 0.84$) with an aspect ratio of six as in Mcalister experiments[4] relative to an inertial reference frame as well as relative to a reference frame fixed to the blade. Figure 8 shows the top view of the roll-up process for $\alpha_0 = 12$ deg ($\lambda \sim 1.26$).

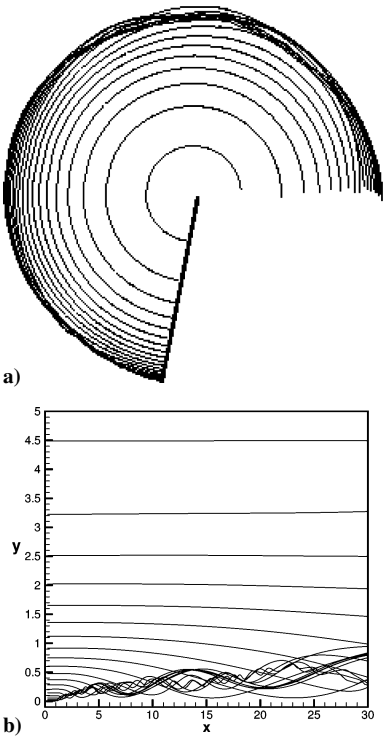

Fig. 7 Comparison of the top view of the roll-up process of trailing vortices shed from a finite-aspect-ratio one-bladed rotor a) relative to an inertial coordinate system (the downstream boundary condition is an infinitely long helix) and b) relative to a coordinate system fixed to the blade. The core radius converges up to $x = 30$. The angle of attack is 8 deg; a single chordwise panel is used.

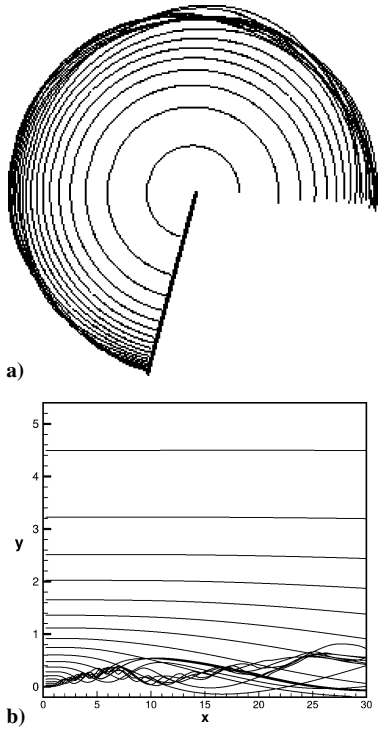

Fig. 8 Comparison of the top view of the roll-up process of trailing vortices shed from a finite-aspect-ratio one-bladed rotor a) relative to an inertial coordinate system (the downstream boundary condition is an infinitely long helix) and b) relative to a coordinate system fixed to the blade. The core radius converges up to $x = 30$. The angle of attack is 12 deg; a single chordwise panel is used.

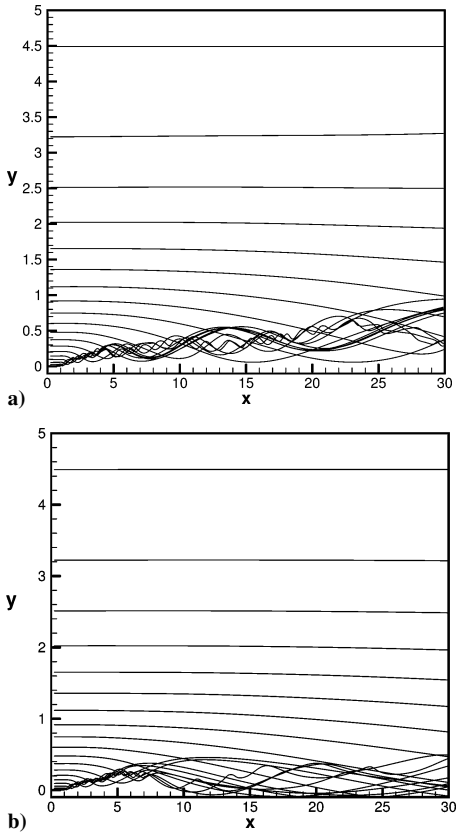

Fig. 9 Comparison of the x–y section view of the roll-up process of trailing vortices shed from a single-bladed finite-aspect-ratio rotor and a single-bladed infinite-aspect-ratio rotor. The core radius has converged up to $x = 30$. A single chordwise panel and 20 spanwise panels were used. The angle of attack is 8 deg, and $\lambda = 0.83$: a) finite-aspect-ratio rotor blade and b) infinite-aspect-ratio rotor blade.

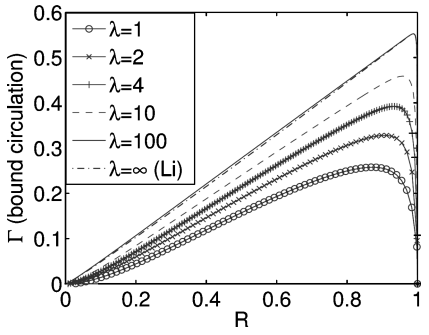

Fig. 10 Comparison of the bound circulation distribution over the entire span for a finite- and an infinite-aspect-ratio rotor blade. The core radius in both cases has converged up to $x = 30$. A single chordwise panel and 20 spanwise panels were used in all cases. The angle of attack is 8 deg.

A comparison of the x–y section view of the roll-over process of the trailing vortices for an infinite-aspect-ratio rotor blade and a finite-aspect-ratio rotor blade is shown in Fig. 9 (relative to the blade). Note that the process of formation of the tip vortex is not very different from that of an infinite-aspect-ratio blade. The only difference is that a larger number of trailing vortices have rolled over at a given downstream distance from the blade tip in the case of the finite blade as compared to the infinite blade; this means that the tip vortex is stronger and moves farther inboard in the former than in the latter. Figure 10 compares the bound circulation distribution on the blade for different values of λ, and it can be seen that there is an increase in the circulation with an increase in the value of λ until a maximum is reached where the circulation distribution becomes the same as that obtained using the lifting-line model.[1]

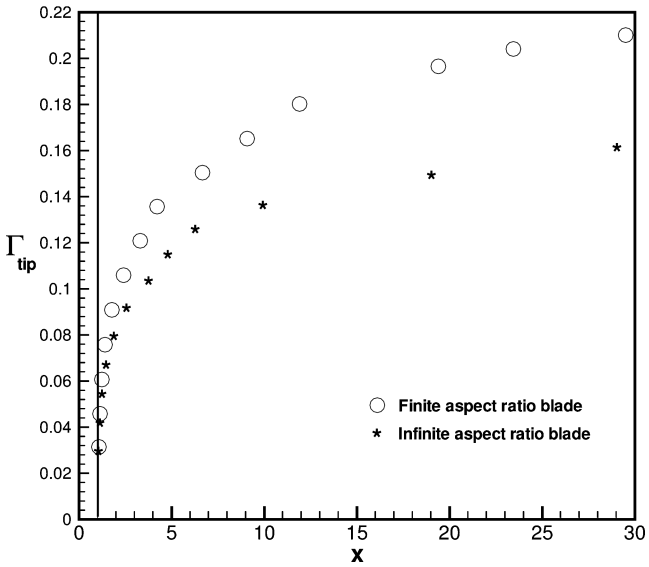

Fig. 11 Comparison of the circulation of the tip vortex for a finite- and infinite-aspect-ratio rotor blade. The core radius in both cases has converged up to $x = 30$. A single chordwise panel and 20 spanwise panels were used in both cases.

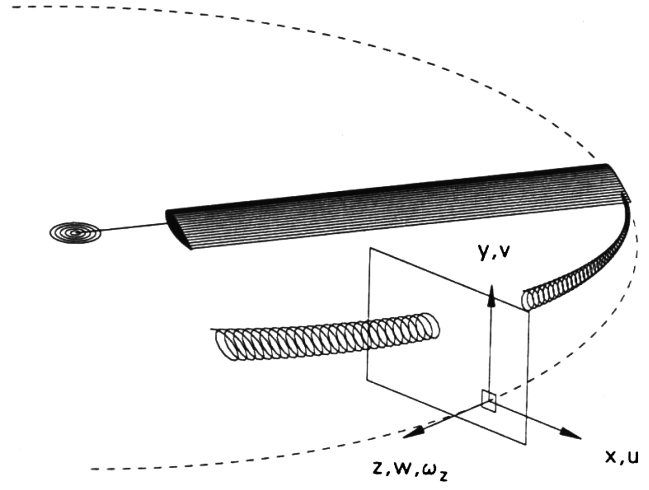

Fig. 12 Experimental configuration for the McAlister et al.[4] experiments. The rotor is rotating counterclockwise when viewed from the top and was a thrust-down experiment. Thus the vortex when viewed from downstream has a clockwise rotation, which is opposite to what is shown in textbooks.

Figure 11 compares the tip circulation of the finite-aspect-ratio blade to that of the infinite-aspect-ratio blade. It is seen that the tip vortex of the former is stronger than that of the latter. This is certainly related to the fact that more trailing vortices have rolled over to form the tip vortex in the case of the finite blade, when compared to the large-aspect-ratio blade. The ratio of the tip-vortex strength to the maximum bound circulation strength for the finite-aspect-ratio blade is 88% while the corresponding value for the very large apsect ratio blade is 91%.

Comparison with Experiments

The experimental results for vertical and horizontal velocity profiles from McAlister et al.[4] were produced for a rotor blade with an aspect ratio of $A = 6$. The coordinate system for the experiments is shown in Fig. 12, and the experimental parameters are presented in Table 1. Note that the notation for the coordinate system is different from that used in the balance of this paper; in this section the McAlister coordinate system is used to present the results. The rotor speed was such that an age of about 30 deg in azimuth corresponds

to about three chord lengths downstream of the trailing edge of the rotor blade. The rotor is rotating counterclockwise when viewed from the top and was a thrust-down experiment. Thus the vortex when viewed from downstream has a clockwise rotation, which is opposite to what is generally shown in textbooks.

We compared the vertical and horizontal velocity profiles across the tip vortex for the finite-aspect-ratio model and the infinite-aspect-ratio or lifting-line model. All of the results shown in this section were produced by evaluating the velocity field at a series of points at the given chordwise location downstream; the grid corresponds to 264 points in the vertical direction and 264 points in the horizontal direction. Of critical importance is the location of the panel edge along the blade span where the velocities are computed. The blade consists of nonuniformly placed spanwise panels along its length. If velocities are computed very close to the panel edges, the velocity shoots up in a discontinuous manner near the panel edge, and a visible hump is seen on the velocity profile. Thus some experimentation in the location of the evaluation points was performed. It was found that the optimal location for the evaluations points in the downstream grid system was midway between the panel edges. Outboard of the blade a uniform grid spacing of (0.01, 0.01) was used. The grid system in the y direction on Fig. 12 is uniform.

As seen in Fig. 13 for the three-chord length location, the finite-aspect-ratio model compares much better than the infinite-aspect-ratio model especially in the outboard region. The infinite-aspect-ratio model compares poorly with experiment particularly in the outboard region, as we go farther downstream at six chord lengths

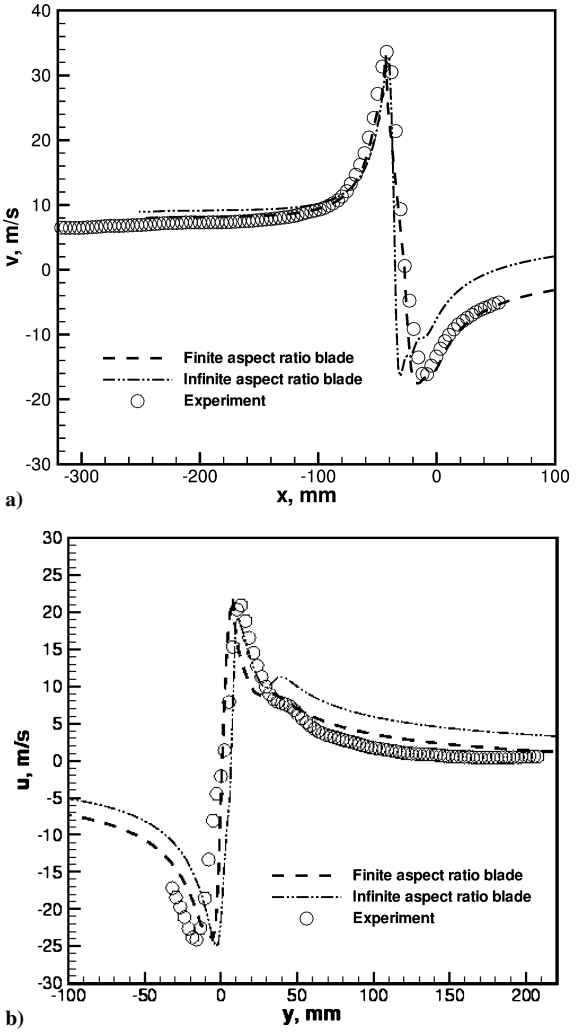

Fig. 13 Comparison of a) vertical velocity profiles and b) horizontal velocity profiles with the experimental results across the tip vortex at a distance of three chord lengths from the trailing edge of the blade: lines, computed results and *, experimental results of McAlister et al.[4]

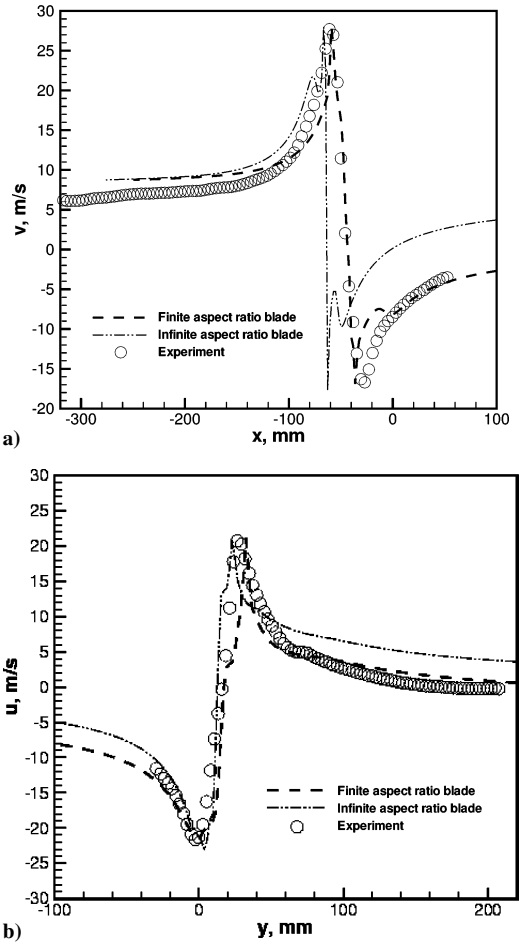

Fig. 14 Comparison of a) vertical velocity profiles and b) horizontal velocity profiles with the experimental results across the tip vortex at a distance of six chord lengths from the trailing edge of the blade: lines, computed results and *, experimental results of McAlister et al.[4]

from the blade tip. However, this does not seem to have an impact on the finite-aspect-ratio model results as seen in Fig. 14. The velocity peaks are very well captured by the finite-aspect-ratio model.

Summary

The current work has focused on the downstream development of the tip vortex for a rotor blade. A lifting surface model complete with an analytical model for the inboard sheet downwash is employed to represent the tip region of the rotor blade, and the roll-up process is used to describe the formation and development of the tip vortex. It is found that the tip vortex does not roll up completely at the trailing edge of the blade as assumed in many wake models; instead, the circulation develops downstream and asymptotes to a nearly constant maximum bound circulation value at some distance downstream greater than 30 chord lengths of the blade. Results were presented for the roll-up structure of the tip vortex.

In this paper, results have been presented for the development of a tip vortex downstream of a finite length and rectangular rotor blade. The results of this lifting surface calculation are qualitatively similar to those presented earlier for the lifting line, but quantitative differences do exist. For example, the finite nature of the blade alters the tip-vortex trajectory, and its circulation is larger, making the finite-blade vortex stronger.

The computational results are compared with experimental data, and the results for both the vertical and horizontal velocities at three and six chords downstream are very good. The comparisons are true predictions because there are no adjustable parameters with which to better fit the data. The experimental comparisons for the finite blade are much better than for the infinite-aspect-ratio blade (lifting-line model) because the structure and trajectory are different

as noted earlier. These results show that at least for this very simple case of a single-bladed, untwisted rotor, a vortex method based on the modified Biot–Savart law can accurately predict the velocity downstream of the rotor. It remains to show that these methods work in the more complex case of a multibladed rotor at full scale.

It might seem surprising that a single chordwise panel is sufficient to accurately represent the vortical flowfield downstream of the rotor blade for this simple case of a rectangular planform. Full-scale rotor blades have planforms much more complicated than this, and in that case it is likely that more chordwise panels will be required. This problem is currently under investigation.

The excellent agreement with experiment has been achieved without the use of a turbulence model, indicating that the influence of turbulent stresses is negligible in the vortex formation process for the parameters of the experiment.

Acknowledgments

This work is supported by the Rotorcraft Center of Excellence at Georgia Institute of Technology and was sponsored by the U.S. Army Research office.

References

[1]Li, H., "The Formation of Rotor Tip Vortices," *Journal of Aircraft*, Vol. 39, No. 5, 2002, pp. 739–749.

[2]Mahalingam, R., "Experiments on the Origin of Tip Vortices," AIAA Paper 2000-0278, Jan. 2000.

[3]Bhagwat, M. J., and Leishman, G. J., "On the Relationship Between Blade Circulation and Tip Vortex Characteristics," *Proceedings of the 54th Forum of the American Helicopter Society*, Vol. 1, American Helicopter Society, Alexandria, VA, 1998, pp. 557–575.

[4]McAlister, K., Tung, C., and Heineck, J. T., "Devices That Alter the Tip Vortex of a Rotor," NASA TM-2001-209625, Aeroflightdynamics Directorate, TR-01-A-003, Feb. 2001.

[5]Ramasamy, M., and Leishman, J. G., "A Reynolds Number Based Rotor Blade Tip Vortex Model," *Proceedings of the 61st Forum of the American Helicopter Society*, American Helicopter Society, Alexandria, VA, 2005.

[6]Conlisk, A. T., "Modern Helicopter Rotor Aerodynamics," *Progress in Aerospace Sciences*, Vol. 37, 2001, pp. 419–476.

[7]Batchelor, G. K., *Introduction to Fluid Dynamics*, Cambridge Univ. Press, Cambridge, England, U.K., 1967, Chap. 7.

[8]McCormick, B. W., Tangler, J. L., and Sherrier, H. E., "Structure of Trailing Vortices," *Journal of Aircraft*, Vol. 5, No. 3, 1968, pp. 260–267.

[9]Brown, C. E., "Aerodynamics of Wake Vortices," *AIAA Journal*, Vol. 11, No. 4, 1973, pp. 531–536.

[10]Moore, D. W., and Saffman, P. G., "The Motion of a Vortex Filament with Axial Flow," *Philosophical Transactions of the Royal Society*, Vol. 272, 1972, pp. 403–429.

[11]Francis, M. S., and Kennedy, D. A., "Formation of a Trailing Vortex," *Journal of Aircraft*, Vol. 16, No. 3, 1978, pp. 148–154.

[12]McAlister, K. W., and Takahashi, R. K., "NACA 0015 Wing Pressure and Trailing Vortex Measurements," NASA TP 3151, Army Aviation Systems Command, TR 91-A-003, Nov. 1991.

[13]Dacles-Mariani, J., Zillac, G. G., Chow, J. S., and Bradshaw, P., "Numerical/Experimental Study of a Wingtip Vortex in the Near Field," *AIAA Journal*, Vol. 33, No. 9, 1995, pp. 1561–1568.

[14]Devenport, W. J., Rife, M. C., Liapis, S. I., and Follin, G. J., "The Structure and Development of a Wing Tip-Vortex," *Journal of Fluid Mechanics*, Vol. 312, 1996, pp. 67–106.

[15]Christopher, M. H., and Lyle, N. L., "Higher-Order Accurate Simulations of Wake and Tip Vortex Flowfields," *Proceedings of the 55th Annual Forum of the American Helicopter Society*, American Helicopter Society, Alexandria, VA, 1999, pp. 1984–1997.

[16]Head, M. R., "Flow Visualization in the Cambridge Univ. Engineering Department," *Flow Visualisation II*, edited by W. Merzkirch, Hemisphere, Washington, DC, 1982, pp. 399–403; also Van Dyke, M., *An Album of Fluid Motion*, Parabolic Press, Stanford, CA, 1982, p. 51.

[17]Anderson, J. D., *Fundamentals of Aerodynamics*, 2nd ed., McGraw–Hill, New York, 1991, Fig. 5.42, p. 366.

[18]Strawn, R. C., "Wing Tip Vortex Calculations with an Unstructured Adaptive-Grid Euler Solver," *Proceedings of the 47th Forum of the American Helicopter Society*, American Helicopter Society, Alexandria, VA, 1991.

[19]Srinivasan, G. R., and Baeder, J. D., "TURNS: A Free-Wake Euler/Navier–Stokes Numerical Method for Helicopter Rotors," *AIAA Journal*, Vol. 31, No. 5, 1993, pp. 959–962.

[20]Wake, B. E., and Choi, D., "Investigation of Higher-Order Upwinded Differencing for Vortex Convection," *AIAA Journal*, Vol. 34, No. 2, 1996, pp. 332–337.

[21]Hariharan, N., and Sankar, L. N., "Higher Order Numerical Simulation of Rotor Flow Field," *Proceedings of the 50th Forum of the American Helicopter Society*, American Helicopter Society, Alexandria, VA, 1994.

[22]Conlisk, A. T., "Modern Helicopter Aerodynamics," *Annual Review of Fluid Mechanics*, Vol. 29, 1997, pp. 515–567.

[23]Cook, C. V., "The Structure of the Rotor Blade Tip Vortex," AGARD, CP-111, Paper 3, Sept. 1972.

[24]Caradonna, F. X., and Tung, C., "Experimental and Analytical Studies of a Model Helicopter Rotor in Hover," NASA TM 81232, Sept. 1981.

[25]Radcliff, T. D., Burggraf, O. R., and Conlisk, A. T., "On the Three-Dimensional Interaction of a Rotor-Tip Vortex with a Cylindrical Surface," *Journal of Fluid Mechanics*, Vol. 425, 2001, pp. 301–334.

[26]Scully, M. P., "A Method of Computing Helicopter Rotor Wake Distortion," Massachusetts Inst. of Technology, ASRL TR 138-1, Cambridge, MA, June 1967.

[27]Miller, W. O., and Bliss, D. B., "Direct Periodic Solutions of Rotor Free Wake Calculations," *Journal of American Helicopter Society*, Vol. 38, No. 2, 1993, pp. 53–60.

[28]Bliss, D. B., Wachspress, D. A., and Quackenbush, T. R., "A New Approach to the Free Wake Problem for Hovering Rotors," *Proceedings of the 41st Annual Forum of the American Helicopter Society*, American Helicopter Society, Alexandria, VA, 1985.

[29]Quackenbush, T. R., Bliss, D. B., and Wachpress, D. A., "Free Wake Analysis of Hover Performance Using a New Influence Coefficient Method," NASA CR-4309, June 1990.

[30]Widnall, S. E., Bliss, D. B., and Zalay, A., "Theoretical and Experimental Study of the Stability of a Vortex Pair," *Aircraft Wake Turbulence and its Detection*, edited by J. Olsen, A. Goldburg, and M. W. Rogers, Plenum, New York, 1971, pp. 305–338.

[31]Kini, S., and Conlisk, A. T., "On the Nature of Locally Steady Rotor Wakes," *Journal of Aircraft*, Vol. 39, No. 5, 2002, pp. 750–758.

[32]Jain, R., and Conlisk, A. T., "Interaction of Tip-Vortices in the Wake of a Two-Bladed Rotor in Axial Flight," *Journal of the American Helicopter Society*, Vol. 45, No. 3, 2000, pp. 157–164.

[33]Falkner, V. M., "The Calculation of Aerodynamic Loading on Surfaces of Any Shape," Aeronautical Research Council, Repts and Memoranda, No. 1910, London, March 1943.

[34]Schlichting, H., and Thomas, H. H. B. M., "Note on the Calculation of Lift Distribution of Swept Wings," Royal Aircraft Establishment, Rept. Aero. 2236, London, 1947.

A. Plotkin
Associate Editor